

引用格式: LI Rongqing, ZHOU Weiwei, TONG Yue, et al. Preparation and Luminescent Properties of Red-emitting $Y_6TeO_{12}:Eu^{3+}$ Phosphor[J]. Acta Photonica Sinica, 2023, 52(2):0216001

李荣青,周薇薇,童悦,等. $Y_6TeO_{12}:Eu^{3+}$ 红色荧光粉的制备与发光特性研究[J]. 光子学报, 2023, 52(2):0216001

$Y_6TeO_{12}:Eu^{3+}$ 红色荧光粉的制备与发光特性研究

李荣青,周薇薇,童悦,郑庆华,吕兆承,赵旺,夏峥嵘,刘芳芳

(淮南师范学院 电子工程学院,淮南 232038)

摘 要:利用高温固相法在 1 200°C 制备了一系列红色荧光粉 $(Y_{1-x})_6TeO_{12}:xEu^{3+}$ ($x=0.1\sim 0.5$) 材料。对样品进行了 X 射线衍射、形貌特征、激发和发射光谱、浓度猝灭、热稳定性、荧光衰减曲线以及发光二极管封装与光色电性能等方面的分析与探究。结果表明:该红色荧光粉样品能被近紫外光(393 nm 处)和蓝光(464 nm 处)有效激发,在 632 nm 处表现出较强的红光发射。根据荧光强度与掺杂浓度的变化趋势,确定出最佳 Eu^{3+} 掺杂量为 $x=0.3$,更多的掺杂量引起浓度猝灭。进一步分析激活剂 Eu^{3+} 间能量传递类型,得出电偶极-电偶极作用导致了浓度猝灭。 $(Y_{0.7})_6TeO_{12}:0.3Eu^{3+}$ 在 150°C 时积分发光强度是室温的 76.5%,热激活能为 0.196 9 eV。该样品的荧光寿命为 813 μs ,色坐标值为(0.637 6, 0.343 1),并基于板上芯片工艺进行了发光二极管封装,对光色电性能进行了表征。 $(Y_{1-x})_6TeO_{12}:xEu^{3+}$ 荧光粉表现出了良好的发光特性、发光热稳定性及色纯度,在白光发光二极管中具有潜在的应用价值。

关键词: $(Y_{1-x})_6TeO_{12}:xEu^{3+}$; 发光特性; 浓度猝灭; 热稳定性; 白光发光二极管

中图分类号: O482.31

文献标识码: A

doi: 10.3788/gzxb20235202.0216001

0 引言

白光发光二极管(Light Emitting Diode, LED)节能高效、低碳环保,在室内外照明、LED 显示屏等领域有着广泛的应用^[1-2]。常用的合成白光 LED 主要采用“蓝光芯片+宽带黄色荧光粉”方案,此组合的不足之处是所合成的白光的相关色温高(CCT~7 000 K)且显色性能偏低(~75)。加入红色荧光粉能有效降低相关色温且实现视觉暖色调照明^[3]。另外,荧光粉性能决定了白光 LED 的发光特征以及显色能力和使用寿命等等^[4],而红色荧光粉在配比中比例高、价格贵。因此,开发制备发光性能优异的新型红色荧光粉材料,是当前荧光材料研究的热点之一^[5]。

当前,开发了许多高效的红色荧光粉材料,例如 Eu^{2+} 掺杂的氮化物和 Mn^{4+} 掺杂的氟化物发光^[6]。尽管许多 Eu^{2+} 激活的氮化物发光具有高的量子效率和出色的热稳定性,但氮化物原料价格昂贵,且合成条件苛刻(高压, ≥ 2.5 MPa; 高温, $\geq 1 500^\circ C$)。典型的 Mn^{4+} 激活氟化物红光材料,例如 $K_2SiF_6:Mn^{4+}$ 和 $K_2TiF_6:Mn^{4+}$ 等,具有高的发光效率^[5,7]。但是,合成氟化物发光需要使用大量的氢氟酸,不仅污染环境,也有害人们的身体健康。一些文献报道了采用低毒的混合酸替代氢氟酸,但替代后材料的发光性能和环境稳定性还有待改善,这就限制了它们的进一步应用^[8]。另外,其他稀土离子激活的氧化物红色发光因其廉价的原料和温和的合成条件而被广泛关注,特别是 Eu^{3+} 激活的氧化物红色发光。这些 Eu^{3+} 激活的红光发光材料具有发射半峰宽窄,色纯度高等优点,但是不能有效地被近紫外或者蓝光激发^[9-10]。在温和的条件下设计合成出可被近紫外或者蓝光有效激发的、高效率及低热猝灭的新型红光荧光粉是一个挑战。

碲酸盐材料具有丰富的构型,碲的四价离子可以构成 TeO_3 、 TeO_4 和 TeO_5 多面体,碲的六价离子可以构

基金项目:安徽高校自然科学基金重点项目(No. KJ2020A0639),安徽省自然科学基金(No. 2108085MB53),校级科研项目(No. 2020XJYB003)

第一作者:李荣青, lrongqing@hnnu.edu.cn

通讯作者:童悦, 22311264@qq.com

收稿日期:2022-08-21; 录用日期:2022-10-14

<http://www.photon.ac.cn>

成 TeO_6 八面体。硝酸盐材料特有的多样性的功能,在多个领域展现了重要的应用价值^[11]。因此,本文开展了 $(\text{Y}_{1-x})_6\text{TeO}_{12}:x\text{Eu}^{3+}$ 红色荧光粉的制备与发光特性探究。

1 实验

1.1 样品制备

采用高温固相反应法制备 $(\text{Y}_{1-x})_6\text{TeO}_{12}:x\text{Eu}^{3+}$ 粉体。所用原料为纯度为99.99%的 Y_2O_3 、 Eu_2O_3 和 TeO_2 ,按照 $(\text{Y}_{1-x})_6\text{TeO}_{12}:x\text{Eu}^{3+}$ (掺杂浓度 $x=0.1\sim 0.5$)化学计量比精确计算并称量。加入适量玛瑙研磨球和无水乙醇在全方位行星式球磨机中球磨4小时,转移至刚玉坩埚后放入高温箱式炉中,在 650°C 温度下预烧10小时。冷却到室温后,将样品加酒精再球磨4小时并在 1200°C 煅烧20小时,冷却到室温后再研磨,可得 $(\text{Y}_{1-x})_6\text{TeO}_{12}:x\text{Eu}^{3+}$ 荧光粉体。

1.2 样品表征

用X射线衍射仪(X Ray Diffraction, XRD)(X-Pert PRO型)对样品进行物相结构分析,辐射源 $\text{Cu-K}\alpha$,扫描步长为 0.02° 。用扫描电子显微镜(Scanning Electron Microscope, SEM)(S-4800型)测量样品形貌。用紫外-可见-近红外分光光度计(UV-3600 Plus型)测试样品的漫反射光谱。用荧光光谱仪(FLS980型)测试样品的荧光寿命。用荧光分光光度计(F-4600型)测试样品的激发、发射光谱。

2 结果与讨论

2.1 物相分析

图1(a)为 $(\text{Y}_{0.7})_6\text{TeO}_{12}:0.3\text{Eu}^{3+}$ 荧光粉的XRD图谱。以 $\text{Y}_6\text{TeO}_{12}$ 为原始模型,使用GSAS-II软件对 $(\text{Y}_{0.7})_6\text{TeO}_{12}:0.3\text{Eu}^{3+}$ 进行Rietveld结构精修^[12]。峰形函数为Pseudo-Voigt函数。在精修过程中设定4a、4b两个结晶学位 Eu^{3+} 按照化学计量比替换 Y^{3+} ,最终精修结果如图1(a)所示。得到图形剩余方差因子 $R_p=4.25\%$,加权图形剩余方差因子 $R_{wp}=5.60\%$,拟合优值(Goodness Of Fit, GOF)为1.60,拟合结果较为理想。从图1(a)可以看出,实验图谱与拟合图谱吻合良好,未观察到杂质衍射峰, Eu^{3+} 取代部分 Y^{3+} 进入晶格并没有改变基质的晶格结构。

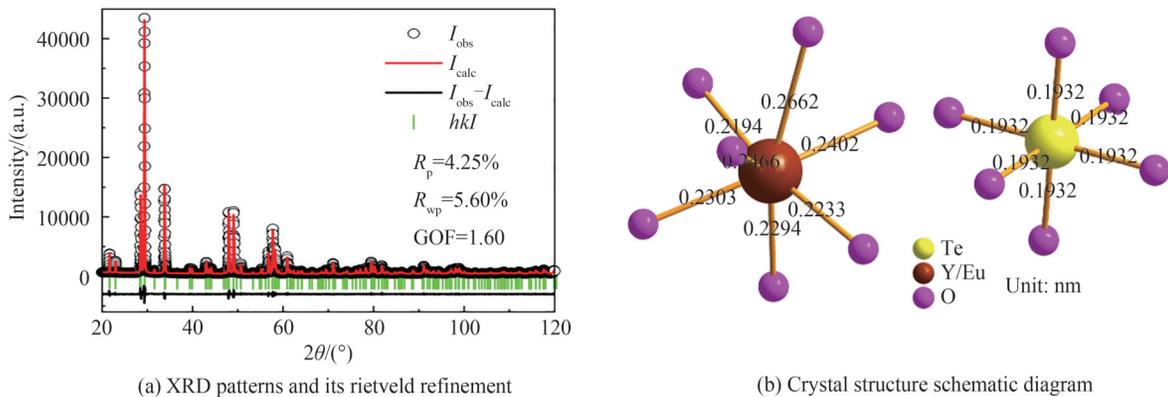


图1 $(\text{Y}_{0.7})_6\text{TeO}_{12}:0.3\text{Eu}^{3+}$ 荧光粉的XRD谱、Rietveld结构精修图和晶体结构示意图

Fig. 1 XRD patterns, rietveld refinement and crystal structure schematic diagram of $(\text{Y}_{0.7})_6\text{TeO}_{12}:0.3\text{Eu}^{3+}$ phosphor

荧光粉 $(\text{Y}_{0.7})_6\text{TeO}_{12}:0.3\text{Eu}^{3+}$ 的空间群为 $R\bar{3}$,属于三方晶系。结晶学参数如乌可夫位置(Wyckoff position)、位置对称性(site symmetry)、原子坐标(atomic coordinates)以及占有率(site occupancy)见表1。精修得到的晶体结构见图1(b)。 $(\text{Y}_{0.7})_6\text{TeO}_{12}:0.3\text{Eu}^{3+}$ 样品中 $\text{Y}^{3+}/\text{Eu}^{3+}$ 周围存在7个 O^{2-} , Te^{6+} 周围存在6个 O^{2-} , $\text{Y}^{3+}/\text{Eu}^{3+}-\text{O}^{2-}$ 键长和 $\text{Te}^{6+}-\text{O}^{2-}$ 键长见图1(b)所示。6个 $\text{Te}^{6+}-\text{O}^{2-}$ 键长均为0.1932 nm,7个 $\text{Y}^{3+}/\text{Eu}^{3+}-\text{O}^{2-}$ 键长均不相同,最短为0.2194 nm,最长则达0.2662 nm。因此, $\text{Y}^{3+}/\text{Eu}^{3+}$ 处于一个高度畸变且无反演中心的配位环境,使得其产生强度大的红光,这对其在白光LED中的应用十分有利。

表1 精修得到的(Y_{0.7})₆TeO₁₂:0.3Eu³⁺荧光粉的原子参数
Table 1 The refined atomic parameters of (Y_{0.7})₆TeO₁₂:0.3Eu³⁺ phosphor

Atom	Wyckoff position	Site symmetry	x/a	y/b	z/c	Site occupancy
Te1	3a	S ₆	0	0	0	1
Eu1	18f	C ₁	0.253 3	0.211 0	0.354 6	0.3
Y1	18f	C ₁	0.253 3	0.211 0	0.354 6	0.7
O1	18f	C ₁	0.183 4	0.142 2	0.109 2	1
O2	18f	C ₁	0.193 5	0.968 6	0.401 4	1

x , y , and z represent the atom positions, and a , b and c denote the lattice parameters

2.2 形貌表征

荧光粉的形貌与封装后的LED器件的光学参数密切相关。图2是(Y_{0.7})₆TeO₁₂:0.3Eu³⁺荧光粉的SEM图片与样品粒径的分布。从图2可以看出,所得的样品颗粒结晶良好,表面较为光滑,光滑表面利于提高发光性能。(Y_{0.7})₆TeO₁₂:0.3Eu³⁺荧光粉颗粒的平均粒径值为4.61 μm,粒径分布在2~8 μm,大部分粉体颗粒的粒径在3.5~6.0 μm之间,样品的颗粒尺寸分布相对均匀。样品颗粒发生的团聚主要是高温烧结或研磨不均匀的原因。

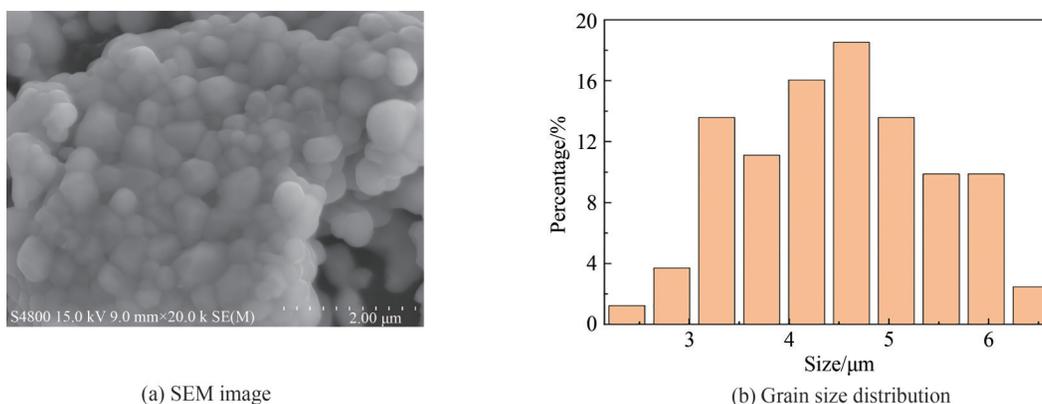


图2 (Y_{0.7})₆TeO₁₂:0.3Eu³⁺荧光粉形貌的SEM图和粒径分布
Fig. 2 SEM image and grain size distribution of (Y_{0.7})₆TeO₁₂:0.3Eu³⁺ phosphor

2.3 漫反射光谱

图3是(Y_{0.7})₆TeO₁₂:0.3Eu³⁺荧光粉的漫反射光谱。在波长小于350 nm的光谱区域存在较强的基质吸收。与Y₆TeO₁₂相比,(Y_{0.7})₆TeO₁₂:0.3Eu³⁺额外增加了Eu³⁺的特征吸收谱线(⁷F₀→⁵D_j, ⁵L_j)。位于362 nm, 382 nm, 393 nm, 414 nm, 465 nm与530 nm波长的锐线激发,属于由Eu³⁺的⁷F₀基态向⁵D₄, ⁵L₇, ⁵L₆, ⁵D₃, ⁵D₂和⁵D₁激发态的电子跃迁^[4]。在393 nm和465 nm处的跃迁,具有较高的吸收强度,说明该样品可以与近紫外或蓝光LED芯片匹配,较为适合蓝光LED芯片泵浦。(Y_{0.7})₆TeO₁₂:0.3Eu³⁺样品在近紫外区具有一定强度的吸收,利用宽而强的电荷迁移带吸收泵浦能量,并将之传递给Eu³⁺,成为增强Eu³⁺发光强度的新渠道。

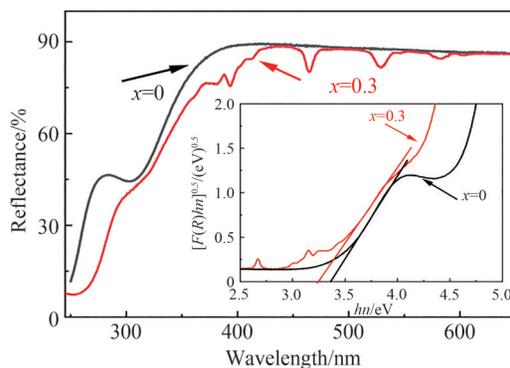


图3 (Y_{0.7})₆TeO₁₂:0.3Eu³⁺样品的漫反射光谱,插图为 $[F(R)hn]^{1/2}-hn$ 曲线
Fig. 3 Diffuse reflection spectra of (Y_{0.7})₆TeO₁₂:0.3Eu³⁺ phosphors. The inset presents curves for $[F(R)hn]^{1/2}$ versus hn

从漫反射光谱可以计算出带隙 E_g ^[13]

$$[F(R)hn]^k = A(hn - E_g) \quad (1)$$

$$F(R) = \frac{(1-R)^2}{2R} \quad (2)$$

式中, A 是一个常数; hn 是光子能量; R 为漫反射率; $F(R)$ 称为 Kubelka-Munk 函数; k 是个常数, 取决于跃迁类型, $k=2/0.5$ 分别对应直接允许和间接允许跃迁类型。尝试 2 种取值后, 发现 $k=0.5$ 时 $[F(R)hn]^{1/2}$ 与 hn 具有良好的线性关系, 如图 3 插图所示, 说明 $(Y_{0.7})_6TeO_{12}:0.3Eu^{3+}$ 荧光粉为间接带隙材料。图 3 中外推直线至横坐标交点处, 可得出纯净和掺 Eu^{3+} 的样品 $(Y_{0.7})_6TeO_{12}:0.3Eu^{3+}$ 的带隙 E_g 分别为 3.36 eV 和 3.25 eV。与同类型掺杂荧光粉如 $Sr_{2-0.21}CdTeO_6:0.14Eu^{3+}$ ($E_g=3.7$ eV)^[14], $NaGdMgTeO_6:Eu^{3+}$ ($E_g=3.58$ eV)^[11] 和 Ca_2CdTeO_6 ($E_g=3.6$ eV)^[14] 等的带隙值接近。

2.4 激发光谱和发射光谱

图 4 左侧曲线是 $(Y_{0.7})_6TeO_{12}:0.3Eu^{3+}$ 样品的激发光谱 (监测波长是 632 nm)。在样品激发光谱中, 有一个紫外区宽的吸收带 (230~300 nm) 和一系列可见区 (360~550 nm) 尖锐的线状激发峰。宽带峰在 263 nm 处出现最强峰, 通过与图 3 的漫反射光谱对比, 可得出 $O^{2-} \rightarrow Eu^{3+}$ 的电荷迁移带产生的激发宽带。尖锐的线状峰是 Eu^{3+} 离子的 4f-4f 组态内电子跃迁, 分别属于 ${}^7F_0 \rightarrow {}^5D_4$ (362 nm), ${}^7F_0 \rightarrow {}^5L_7$ (382 nm), ${}^7F_0 \rightarrow {}^5L_6$ (393 nm), ${}^7F_0 \rightarrow {}^5D_3$ (414 nm), ${}^7F_0 \rightarrow {}^5D_2$ (465 nm) 和 ${}^7F_0 \rightarrow {}^5D_1$ (530 nm) 的电子跃迁^[14-15], 这与图 3 样品的漫反射光谱分析的结果一致。393 nm (${}^7F_0 \rightarrow {}^5L_6$) 处的最强的激发峰位于近紫外区, 另外 465 nm (${}^7F_0 \rightarrow {}^5D_2$) 处较强激发峰, 与蓝光芯片的发射相符合。说明 $(Y_{0.7})_6TeO_{12}:0.3Eu^{3+}$ 样品能够被近紫外或蓝光 LED 芯片有效激发, 适用于白光 LED 的红色发光组分。

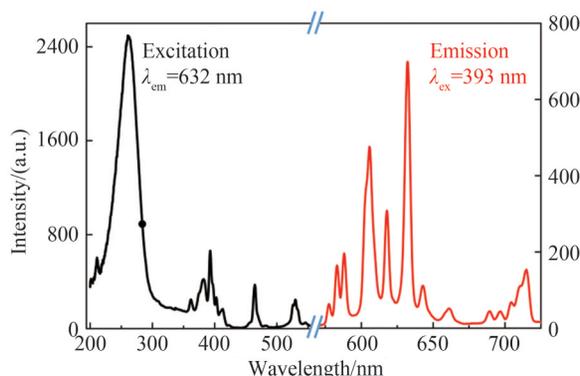


图 4 $(Y_{0.7})_6TeO_{12}:0.3Eu^{3+}$ 样品的激发光谱 (左侧黑色实线, $\lambda_{em}=632$ nm)、发射光谱 (右侧红色实线, $\lambda_{ex}=393$ nm)

Fig. 4 Excitation (left black line, $\lambda_{em}=632$ nm) and emission (right red line, $\lambda_{ex}=393$ nm) spectra of $(Y_{0.7})_6TeO_{12}:0.3Eu^{3+}$ phosphors

图 4 右侧是 $(Y_{0.7})_6TeO_{12}:0.3Eu^{3+}$ 荧光粉 (激发光波长 393 nm) 的发射光谱图。发射光谱由 5 组发射带组成, 分别对应 Eu^{3+} 离子的 ${}^5D_0 \rightarrow {}^7F_0$ (578 nm), ${}^5D_0 \rightarrow {}^7F_1$ (585 nm), ${}^5D_0 \rightarrow {}^7F_2$ (616 nm), ${}^5D_0 \rightarrow {}^7F_3$ (660 nm) 和 ${}^5D_0 \rightarrow {}^7F_4$ (710 nm) 跃迁。其中 ${}^5D_0 \rightarrow {}^7F_1$, ${}^5D_0 \rightarrow {}^7F_2$ 和 ${}^5D_0 \rightarrow {}^7F_4$ 的跃迁发射出现劈裂现象。 Eu^{3+} 离子的发射光谱的行为, 其对所处晶格格位的对称性非常敏感。 Eu^{3+} 若处于较低对称性的格位时, 7F_j 能级简并解除, 产生较多能级劈裂。本工作中 Eu^{3+} 在 Y_6TeO_{12} 中取代的 Y^{3+} 处于较低的对称格位 (见 2.1 节物相分析的讨论), 环境的影响使得发射峰中出现了劈裂^[1,11]。 Eu^{3+} 周围晶体场环境对 ${}^5D_0 \rightarrow {}^7F_j$ 跃迁的数量和强度影响很大。当 Eu^{3+} 离子处于基质中心对称格位时, 主要是 ${}^5D_0 \rightarrow {}^7F_1$ 的磁偶极电子跃迁。 ${}^5D_0 \rightarrow {}^7F_2$ 跃迁发射位于 605~640 nm 波长区间, 在样品 $Ln_6XO_{12}:Eu^{3+}$ (Ln 为 Gd, Lu; X 为 Mo, W) 中也具有相似的发射特征^[16]。该现象产生的根源在于 Eu^{3+} 在该类基质中的位置对称性较低 (位置对称群 C_1), 处在无反演对称的晶体场环境中, 且晶体场能级分裂较大。当 Eu^{3+} 离子在基质晶体中占据非对称格位时, ${}^5D_0 \rightarrow {}^7F_2$ 的电偶极跃迁占主导。不对称比率 $R = I({}^5D_0 \rightarrow {}^7F_2)/I({}^5D_0 \rightarrow {}^7F_1)$ 常用于判断 Eu^{3+} 离子占据格位的对称性, I 为积分发光强度。 $(Y_{0.7})_6TeO_{12}:0.3Eu^{3+}$ 样品的 R 值为 6.338, ${}^5D_0 \rightarrow {}^7F_2$ 电偶极跃迁在发射光谱中占据主导地位, 由此可以推断 Eu^{3+} 位于非对称中心晶体场中, 这与 2.1 节 $(Y_{0.7})_6TeO_{12}:0.3Eu^{3+}$ 荧光粉结构的物相分析相吻合。高于文献中的铋酸盐 $Ba_{0.9}LaLiTeO_6:0.1Eu^{3+}$ ($R=4.11$)^[17]、钛酸盐 $La_{1.6}ZnTiO_6:0.4Eu^{3+}$ ($R=3.10$)^[3]、铌酸盐 $Y_{0.5}Lu_{0.5}NbO_4:5\%Eu^{3+}$

($R=5.02$)^[18]和铋酸盐 CaLa_{0.5}MgSbO₆:0.5Eu³⁺ ($R=5.90$)^[19], 大的 R 值有利于提高红光强度和色纯度^[3]。

样品 (Y_{1-x})₆TeO₁₂:xEu³⁺ 中, Eu³⁺ 作为发光中心, 其含量与样品的发射光谱的强度密切相关。测试了一系列不同 Eu³⁺ 浓度掺杂下 (Y_{1-x})₆TeO₁₂:xEu³⁺ 的发射光谱, 激发光波长均为 393 nm, 如图 5 所示, 插图为积分发光强度随样品掺杂浓度 x 的变化。从图 5 中可以发现, (Y_{1-x})₆TeO₁₂:xEu³⁺ 样品发射光谱的形状及谱峰位置基本不变, 只是发光强度随 Eu³⁺ 浓度的增加先增强后减小, 当 Eu³⁺ 掺杂浓度为 30% ($x=0.3$) 时达到最大。因此在基质 Y₆TeO₁₂ 中, Eu³⁺ 离子的最佳掺杂浓度为 30%。

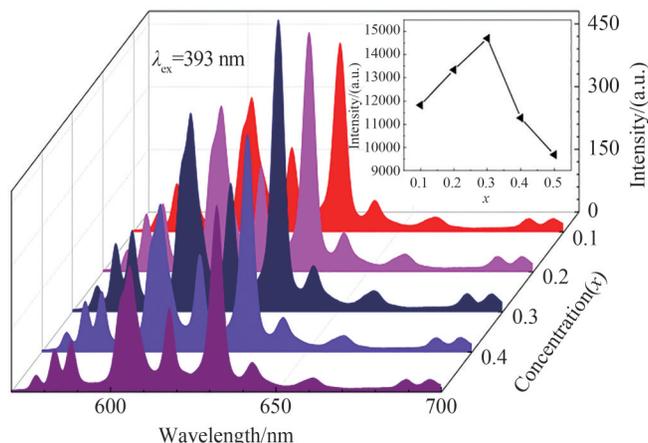


图 5 五种掺杂浓度 (Y_{1-x})₆TeO₁₂:xEu³⁺ ($x=0.1\sim 0.5$) 样品的发射光谱图 ($\lambda_{\text{ex}}=393$ nm), 插图为积分发光强度与掺杂浓度 x 之间的关系

Fig. 5 Emission spectra of (Y_{1-x})₆TeO₁₂:xEu³⁺ with different doping concentrations ($x=0.1\sim 0.5$, $\lambda_{\text{ex}}=393$ nm), the inset shows the relationship between integral luminescence intensity and doping concentrations x

当 Eu³⁺ 离子浓度较小时, 相邻粒子中心间距离较大, 将吸收的大部分能量以辐射跃迁的形式释放。在 x 从 0.1 增大到 0.3 的过程中, 随着 Eu³⁺ 离子浓度的增加, 发光中心增多, 发光强度增大; 在 x 超过 0.3 之后, 继续增大 x 会出现 Eu³⁺ 的浓度猝灭现象。这种浓度猝灭现象出现的可能原因有辐射再吸收作用、交换相互作用或电多极-电多极相互作用。当发射光谱与激发光谱大量重叠时, 离子间的能量传递为辐射再吸收作用。由图 4 样品的激发光谱、发射光谱可知, (Y_{1-x})₆TeO₁₂:xEu³⁺ 样品的激发光谱与发射光谱无明显重叠现象, 所以 Eu³⁺ 之间的无辐射能量传递不可能是基于该作用。

(Y_{1-x})₆TeO₁₂:xEu³⁺ 样品中 Eu³⁺ 能量传递临界距离 (R_c) 可表达为^[20]

$$R_c = 2 \left(\frac{3V}{4\pi x_c N} \right)^{\frac{1}{3}} \quad (3)$$

式中, N 代表晶胞中稀土离子的数目, x_c 为激活剂最佳掺杂浓度, V 表示晶胞体积。在 (Y_{0.7})₆TeO₁₂:0.3Eu³⁺ 晶体中, $N=18$, $x_c=0.3$, $V=0.78453$ nm³, 计算得到 Eu³⁺ 在 (Y_{1-x})₆TeO₁₂:xEu³⁺ 中的能量传递临界距离为 0.652 nm。交换相互作用发生的前提是 $R_c \leq 0.5$ nm^[21], 所以 (Y_{1-x})₆TeO₁₂:xEu³⁺ 样品的浓度猝灭并非离子间的交换相互作用导致。可以推断, Eu³⁺ 的浓度猝灭现象是由电多极-电多极作用造成的。

为了进一步探究这种电多极-电多极相互作用, 在 Eu³⁺ 掺杂浓度 x 大于猝灭浓度时, 积分发光强度 I 与掺杂浓度 x 之间的关系可表达为^[22]

$$\frac{I}{x} \approx Kx^{-\frac{Q}{3}} \quad (4)$$

式中, I 为发射光谱在 550~700 nm 区间中的积分强度, K 在同种晶体结构的相同激发条件下为常数, x 为激活剂离子掺杂浓度。Eu³⁺ 之间的电多极-电多极作用类型可通过 Q 指数确定。 $Q=6, 8$ 或 10 , 表示电偶极-电偶极、电偶极-电四极、电四极-电四极之间的作用。图 6 为 (Y_{1-x})₆TeO₁₂:xEu³⁺ 的发光积分强度与掺杂浓度的关系, $\lg(I/x)$ 与 $\lg x$ 在 $x=0.3$ 后呈线性依赖关系, 斜率为 -1.819, $Q=5.457$, 该值接近 6。因此, 在 (Y_{1-x})₆TeO₁₂:xEu³⁺ 样品中, Eu³⁺ 离子间产生的浓度猝灭现象主要是基于电偶极-电偶极作用。在很多掺杂 Eu³⁺ 离子的荧光粉中有此电偶极-电偶极作用机制, 如 Sr₂MgTeO₆:Eu³⁺、La₂MgTiO₆:Eu³⁺、LiSrBiTeO₆:

Eu^{3+} 、 NaMgLaTeO_6 : Eu^{3+} 和 NaMgGdTeO_6 : Mn^{4+} 等^[20,23-24]。

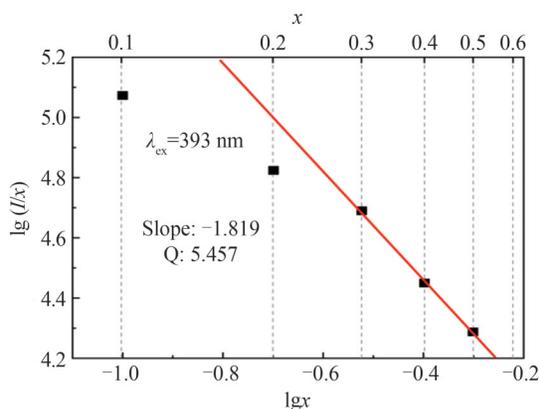


图6 积分发光强度 I 、掺杂浓度 x 之间的 $\lg(I/x)$ 与 $\lg x$ 的关系

Fig. 6 The relationship between $\lg(I/x)$ and $\lg x$ of integral luminescence intensity I and doping concentrations x

2.5 发光热稳定性

在白光LED的实际使用中,一般在连续发光半小时后,整个LED芯片的温度可以升高到 $100\sim 200^\circ\text{C}$,使荧光粉产生温度猝灭效应^[22]。为了分析 $(\text{Y}_{0.7})_6\text{TeO}_{12}:0.3\text{Eu}^{3+}$ 荧光粉材料的热稳定性,测试了在 $18^\circ\text{C}\sim 200^\circ\text{C}$ 温度范围内样品的发射光谱,如图7所示。随着样品温度逐渐升高, $(\text{Y}_{0.7})_6\text{TeO}_{12}:0.3\text{Eu}^{3+}$ 的发光强度逐渐下降。在 150°C 时样品的积分发光强度是室温的76.5%,当温度升高到 200°C 时,样品积分发光强度降低了约30%。

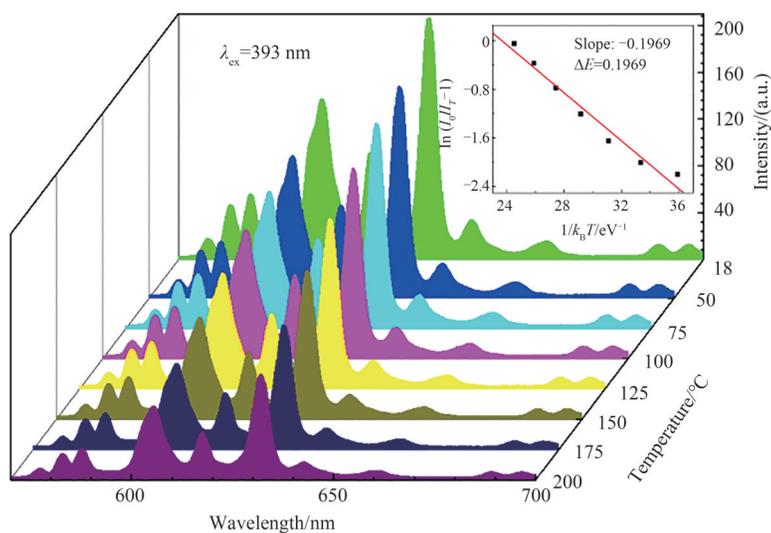


图7 不同工作温度下 $(\text{Y}_{0.7})_6\text{TeO}_{12}:0.3\text{Eu}^{3+}$ 荧光粉的发射光谱(插图为 $\ln[I_0/I_T-1]$ 和 $1/(k_B T)$ 之间的关系)

Fig. 7 Emission spectra of $(\text{Y}_{0.7})_6\text{TeO}_{12}:0.3\text{Eu}^{3+}$ phosphors at different temperatures (the inset shows the relationship between $\ln[I_0/I_T-1]$ and $1/(k_B T)$)

研究表明发光强度 I_T 随温度的变化满足^[1]

$$I_T = \frac{I_0}{1 + A \exp\left(-\frac{\Delta E}{k_B T}\right)} \quad (5)$$

式中, A 是常数, ΔE 是温度猝灭中的热激活能, k_B 是玻尔兹曼常数, T 为绝对温度, I_0 是样品在室温的发光强度。将式(5)两边取对数得

$$\ln\left(\frac{I_0}{I_T} - 1\right) = -\frac{\Delta E}{k_B T} + \ln A \quad (6)$$

通过作图(图7中插图),可计算得到热激活能为 $\Delta E=0.1969\text{ eV}$ 。其值与商用红色荧光粉 $\text{Sr}_2\text{Si}_5\text{N}_8:\text{Eu}^{2+}$

($\Delta E=0.2$ eV)^[14]接近,介于其它文献中荧光粉激活能值之间,如CaLa_{0.5}MgSbO₆:0.5Eu³⁺ ($\Delta E=0.173$ eV)^[19], La_{1.6}ZnTiO₆:0.4Eu³⁺ ($\Delta E=0.193$ eV)^[3], LiLa_{0.7}MgWO₆:0.3Eu³⁺ ($\Delta E=0.225$ eV)^[25], Ca₂Lu_{0.6}TaO₆:0.4Eu³⁺ ($\Delta E=0.242$ eV)^[1],说明(Y_{0.7})₆TeO₁₂:0.3Eu³⁺荧光粉具有良好的热稳定性,可作为白光LED的候选材料。

2.6 荧光衰减曲线

荧光寿命反映了荧光粉晶体场结构和发光离子所处局域环境的变化,是衡量荧光粉发光性能的重要指标之一。图8为不同浓度Eu³⁺离子掺杂下(Y_{1-x})₆TeO₁₂:xEu³⁺荧光粉⁵D₀→⁷F₂跃迁的荧光衰减曲线,激发光波长393 nm,监测波长为632 nm。尝试了单指数、双指数两种拟合方式,发现5种样品的荧光衰减曲线均可以用双指数拟合,拟合公式为

$$I(t) = I_0 + A_1 e^{-t/\tau_1} + A_2 e^{-t/\tau_2} \quad (7)$$

式中, $I(t)$ 是样品的发光强度, t 表示时间, τ_1 和 τ_2 分别表示第1和第2个指数分量的荧光衰减时间, A_1 与 A_2 是常数。综合考虑2个荧光衰减时间,样品荧光有效寿命计算公式为^[2]

$$\tau_{\text{eff}} = \frac{A_1 \tau_1^2 + A_2 \tau_2^2}{A_1 \tau_1 + A_2 \tau_2} \quad (8)$$

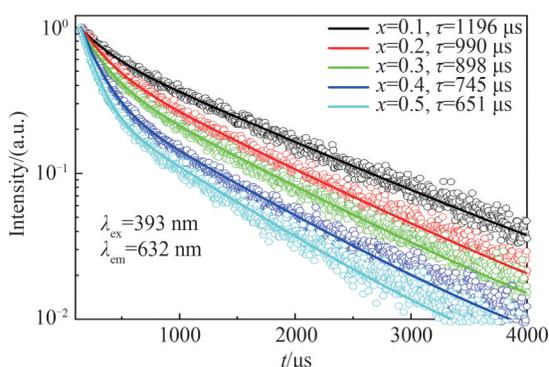


图8 荧光粉(Y_{1-x})₆TeO₁₂:xEu³⁺的荧光衰减曲线
Fig. 8 Decay curves of (Y_{1-x})₆TeO₁₂:xEu³⁺ phosphors

五种Eu³⁺离子掺杂浓度下的荧光衰减曲线,双指数拟合的相关系数均在99.95%以上。拟合所得 τ_1 和 τ_2 差别较大,这说明(Y_{1-x})₆TeO₁₂:xEu³⁺材料存在两种发光中心,短寿命 τ_1 是以非辐射方式(缺陷捕获、电子转移等等)复合为主,长寿命 τ_2 是以辐射方式复合为主^[26]。通过式(8)计算出的有效寿命分别是1114 μ s, 907 μ s, 813 μ s, 661 μ s, 583 μ s。随着Eu³⁺离子掺杂浓度的增加,样品(Y_{1-x})₆TeO₁₂:xEu³⁺材料的短寿命 τ_1 先基本不变后逐渐降低,同时长寿命 τ_2 逐渐降低,其有效荧光寿命逐渐降低。在2.1节样品结构的物相分析和2.4节激发光谱和发射光谱分析中可知,掺杂离子Eu³⁺位于非对称中心晶体场中。由于Eu³⁺离子掺入,晶体场的非对称性增加,导致此阶段以辐射复合为主的长寿命 τ_2 逐渐减小^[11]。而随着Eu³⁺离子浓度的增加,Eu³⁺离子之间的距离变短,离子之间产生了无辐射能量传递过程,此阶段样品的发光强度逐渐降低(见2.4节处样品的发射光谱强度随掺杂浓度的变化)。该无辐射能量传递过程增加了掺杂离子Eu³⁺的⁵D₀能级上粒子的去布居通道,使得样品非辐射方式的短寿命 τ_1 和辐射复合方式的长寿命 τ_2 逐渐降低,导致了⁵D₀能级的有效寿命逐渐减小。

荧光粉的量子效率 η 反映了荧光粉将吸收的光能转变成发光的本领。量子效率可以利用发射光谱与荧光寿命,通过Judd-Ofelt理论计算得出。Eu³⁺离子的⁵D₀→⁷F_J($J=0\sim 4$)能级跃迁中,其跃迁类型分别是: $J=0, 3$ 为禁戒, $J=1$ 为磁偶极, $J=2, 4$ 为电偶极。利用图4的发射光谱和图8得出的荧光寿命,详细的Judd-Ofelt计算过程见参考文献^[27],计算结果列于表2。可以看出,样品(Y_{0.7})₆TeO₁₂:0.3Eu³⁺的计算量子效率 η 为72.5%, Ω_2 值达到 10.2×10^{-20} cm²,较大的 Ω_2 值反映了Eu³⁺--O²⁻键较高的共价性,有利于⁵D₀→⁷F₂发光强度的提高。这些数据结果直观的显示了所得样品(Y_{0.7})₆TeO₁₂:0.3Eu³⁺具有一定的应用潜能。

表3给出了一些有代表性结构的红色荧光粉的发光特征参数。样品(Y_{0.7})₆TeO₁₂:0.3Eu³⁺的合成温度适中(1200℃),与钛、钨酸盐相当,低于钽、铋、铌酸盐(约1500℃),减轻了对合成制备的设备要求且能节约能源。荧光寿命与钨酸盐Ca₂La_{0.5}SbO₆:0.5Eu³⁺相当,高于钛酸盐La_{1.6}ZnTiO₆:0.4Eu³⁺、钨酸盐LiLa_{0.7}MgWO₆:0.3Eu³⁺、钽酸盐Ca₂Lu_{0.6}TaO₆:0.4Eu³⁺、铌酸盐Y_{0.5}Lu_{0.5}NbO₄:5%Eu³⁺和碲酸盐Ba_{0.9}LaLiTeO₆:0.1Eu³⁺

表2 样品 $(Y_{0.7})_6TeO_{12}:0.3Eu^{3+}$ 的 Judd-Ofelt 计算结果
Table 2 Judd-Ofelt analysis of $(Y_{0.7})_6TeO_{12}:0.3Eu^{3+}$

Wavelength λ /nm	Radiative transition rate A/s^{-1}	Radiative lifetime $\tau_r/\mu s$	Measured lifetime $\tau_f/\mu s$	Quantum efficiency η
577	14.6	1 122.1	813.2	72.5%
588	100.5			
632	620.8			
661	26.5			
725	128.8			

$\Omega_2=10.2 \times 10^{-20} \text{ cm}^2$ $\Omega_4=4.3 \times 10^{-20} \text{ cm}^2$

(500 μs 左右)。其不对称比率 R 低于钨酸盐 $LiLa_{0.7}MgWO_6:0.3Eu^{3+}$ 和铌酸盐 $BaLa_{0.7}MgNbO_6:0.3Eu^{3+}$, 高于铋酸盐 $Ba_{0.9}LaLiTeO_6:0.1Eu^{3+}$ 、钛酸盐 $La_{1.6}ZnTiO_6:0.4Eu^{3+}$ 、铌酸盐 $Y_{0.5}Lu_{0.5}NbO_4:5\%Eu^{3+}$ 和铋酸盐 $CaLa_{0.5}MgSbO_6:0.5Eu^{3+}$ 。主要是由于三方晶系的 $(Y_{0.7})_6TeO_{12}:0.3Eu^{3+}$ 中 Eu^{3+} 所处格位配体多面体对称性较低(C1点群), 有利于增强 ${}^5D_0 \rightarrow {}^7F_2$ 超灵敏跃迁发射, 因此不对称比率 R 较高, 红色色纯度更大。整体而言, $(Y_{0.7})_6TeO_{12}:0.3Eu^{3+}$ 发光特性良好, 这促使我们进一步对其进行LED封装和光色电性能的研究。

表3 Eu^{3+} 激活荧光粉的光学性能比较
Table 3 Luminescence properties comparison of some Eu^{3+} activated phosphors

Phosphor	Sintered temperature / $^{\circ}C$	Asymmetric ratio	Luminescence lifetimes / μs	Activation energy / eV	Reference
$Sr_{1.5}Na_{0.25}MgTeO_6:0.25Eu^{3+}$	1 100	7.47	—	0.270	[24]
$Ba_{0.9}LaLiTeO_6:0.1Eu^{3+}$	800	4.11	550	—	[17]
$La_{1.6}ZnTiO_6:0.4Eu^{3+}$	1 200	3.10	544	0.193	[3]
$LiLa_{0.7}MgWO_6:0.3Eu^{3+}$	1 200	10.0	450	0.225	[25]
$Ca_2Lu_{0.6}TaO_6:0.4Eu^{3+}$	1 500	—	580	0.242	[1]
$Y_{0.5}Lu_{0.5}NbO_4:5\%Eu^{3+}$	1 450	5.02	650	—	[18]
$Ca_2La_{0.5}SbO_6:0.5Eu^{3+}$	1 500	—	927	0.211	[28]
$BaLa_{0.7}MgNbO_6:0.3Eu^{3+}$	1 450	12	—	0.270	[29]
$CaLa_{0.5}MgSbO_6:0.5Eu^{3+}$	1 450	5.90	—	0.173	[19]
$(Y_{0.7})_6TeO_{12}:0.3Eu^{3+}$	1 200	6.338	813	0.196 9	This work

2.7 LED封装与光色电性能

色品坐标是反映荧光粉的发光性能的重要参数之一。利用样品的发光光谱计算了 $(Y_{0.7})_6TeO_{12}:0.3Eu^{3+}$ 的色坐标值, 见图9插图。 $(Y_{0.7})_6TeO_{12}:0.3Eu^{3+}$ 样品的红色区色坐标值为(0.637 6, 0.343 1), 与美国国家电视

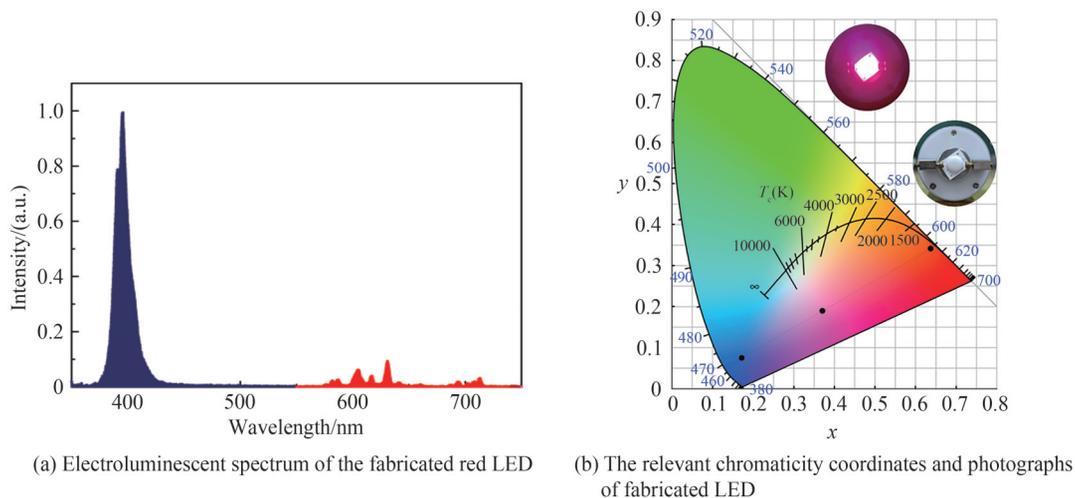


图9 所制备的红光LED的电致发光光谱、色坐标图和LED照片

Fig. 9 Electroluminescent spectrum, relevant chromaticity coordinates and photographs of the fabricated red LED

标准委员会下的标准值(0.670,0.330)接近。相关色温(Correlated Color Temperature, CCT)是黑体温度,是光源发光时的颜色与黑体加热到某一温度的颜色相同时黑体此时的温度。其计算方法如式(9)所示^[11]。

$$CCT = -449n^3 + 3525n^2 - 6823.3n + 5520.33 \quad (9)$$

式中, $n=(x-x_e)/(y-y_e)$,其中 (x, y) 为光源所产生光谱对应的色坐标值, (x_e, y_e) 等于(0.332 0,0.185 8)是中心坐标。计算后(Y_{0.7})₆TeO₁₂:0.3Eu³⁺样品的相关色温为2 276 K,与NaGdMgTeO₆:Eu³⁺(CCT=2 227 K)^[11]的相关色温接近。相关色温值低于3 000 K以下,表明荧光粉更适用于暖型白光LED。为了进一步分析(Y_{0.7})₆TeO₁₂:0.3Eu³⁺荧光粉材料的显色性能,采用式(10)对色纯度进行了计算^[30]。

$$\text{Color purity} = \sqrt{\frac{(x-x_i)^2 + (y-y_i)^2}{(x_d-x_i)^2 + (y_d-y_i)^2}} \quad (10)$$

式中, (x, y) 为(Y_{0.7})₆TeO₁₂:0.3Eu³⁺材料的色坐标; (x_i, y_i) 为国际照明委员会规定的白光的坐标值,为(0.310,0.316); (x_d, y_d) 为主波长坐标值,为(0.672,0.328)。经计算,(Y_{0.7})₆TeO₁₂:0.3Eu³⁺材料的色纯度为92.5%,高于LiPbB₅O₉:xEu³⁺、NaTb_{1-x}F₄:xEu³⁺等荧光粉材料^[31-32]。在2.4部分的讨论中,(Y_{0.7})₆TeO₁₂:0.3Eu³⁺材料的不对称比率 R 为6.338,大的 R 值使得样品具有了较好的色纯度。这些结果表明,荧光粉(Y_{0.7})₆TeO₁₂:0.3Eu³⁺具有良好的显色性和适宜的色温。为了验证所制备的荧光粉的潜在应用,将(Y_{0.7})₆TeO₁₂:0.3Eu³⁺样品样品与硅胶均匀混合后涂覆芯片上,用板上芯片(Chip On Board, COB)形式封装成红色LED灯珠。在25 mA正向电流驱动下,灯珠发出红光(见图9插图)。样品的电致发光光谱(图9)中,360~440 nm处的发射带由近紫外芯片产生,560~740 nm处的发射带归属于样品发光。灯珠色品坐标值为(0.379 3,0.179 6),3个色坐标位于一条直线上,与混光原理相符合。

3 结论

本文利用高温固相法制备了一系列(Y_{1-x})₆TeO₁₂:xEu³⁺荧光粉,对其粉体结构、形貌、发光特性、浓度猝灭机理、能量传递效应、发光热稳定性、荧光衰减曲线和量子效率以及LED封装与光色电性能进行了分析。XRD结果表明,(Y_{1-x})₆TeO₁₂:xEu³⁺荧光粉具有单一晶相,Eu³⁺作为激活剂和敏化剂进入Y₆TeO₁₂晶格中。SEM结果表明,粉体颗粒结晶良好,形貌规则,大部分颗粒的尺寸集中在3.5~6 μm之间。通过漫反射光谱计算出带隙为3.25 eV。在393 nm紫外光激发下,发射光谱由5组发射带组成,以⁵D₀→⁷F₂跃迁为主,发光不对称比率 $R=I(^5D_0 \rightarrow ^7F_2)/I(^5D_0 \rightarrow ^7F_1)$ 为6.338。通过Eu³⁺掺杂量对(Y_{1-x})₆TeO₁₂:xEu³⁺荧光粉发光强度的影响,得出Eu³⁺离子的最佳掺杂浓度为30%($x=0.3$),并证实了浓度猝灭由电偶极-电偶极作用造成。分析荧光粉的发光热稳定性,计算得到Eu³⁺离子的热激活能为0.196 9 eV。(Y_{1-x})₆TeO₁₂:xEu³⁺荧光粉的荧光衰减曲线则符合双指数衰减模型,随着Eu³⁺离子掺杂浓度的提高,荧光寿命逐渐缩短。(Y_{0.7})₆TeO₁₂:0.3Eu³⁺样品的荧光寿命为813 μs。另外,完成了基于COB工艺的红光LED封装,并对其光色电性能进行了初步的表征。综上所述,(Y_{1-x})₆TeO₁₂荧光粉具备较好的晶体结构、发光特征以及温度猝灭小等优点,有望成为一种新型白光LED用红色荧光粉的候选材料。

参考文献

- [1] SUN Q, WANG S, DEVAKUMAR B, et al. Double perovskite Ca₂LuTaO₆:Eu³⁺ red-emitting phosphors: synthesis, structure and photoluminescence characteristics[J]. Journal of Alloys and Compounds, 2019, 804: 230-236.
- [2] LIANG Dongbao, ZHANG Rui, SHEN Yufang, et al. Synthesis and luminescent properties of BaLaGa₃O₇:Bi³⁺ phosphors[J]. Acta Photonica Sinica, 2022, 51(3): 0316002.
梁冬宝,张瑞,申玉芳,等. BaLaGa₃O₇:Bi³⁺荧光粉的制备及发光性能研究[J]. 光子学报, 2022, 51(3): 0316002.
- [3] FU A, GUAN A, GAO F, et al. A novel double perovskite La₂ZnTiO₆:Eu³⁺ red phosphor for solid-state lighting: Synthesis and optimum luminescence[J]. Optics & Laser Technology, 2017, 96: 43-49.
- [4] ZHAO Wang, ZHOU Weiwei, LIU Shuhe, et al. Luminescent characters and energy transfer mechanisms of BaGd₂(MoO₄)₄:Tb³⁺, Eu³⁺ Phosphors[J]. Chinese Journal of Luminescence, 2019, 40(5): 581-588.
赵旺,周薇薇,刘淑河,等. BaGd₂(MoO₄)₄:Tb³⁺, Eu³⁺荧光粉的发光特性与能量传递机理[J]. 发光学报, 2019, 40(5): 581-588.
- [5] HUANG L, LIU Y, YU J, et al. Highly stable K₂SiF₆:Mn⁴⁺@K₂SiF₆ composite phosphor with narrow red emission for white leds[J]. ACS applied materials & interfaces, 2018, 10(21): 18082-18092.
- [6] DING X, WANG Y. Commendable Eu²⁺-doped oxide-matrix-based LiBa₁₂(BO₃)₇F₄ red broad emission phosphor excited

- by NUV light: electronic and crystal structures, luminescence properties[J]. ACS Applied Materials & Interfaces, 2017, 9(28): 23983-23994.
- [7] HUANG L, LIU Y, SI S, et al. A new reductive DL-mandelic acid loading approach for moisture-stable Mn⁴⁺ doped fluorides[J]. Chemical Communications, 2018, 54(84): 11857-11860.
- [8] ZHU Y, YUAN S, HUANG L, et al. Optimizing and adjusting the photoluminescence of Mn⁴⁺-doped fluoride phosphors via forming composite particles[J]. Dalton Transactions, 2019, 48(2): 711-717.
- [9] ZHAO Cong, MENG Qingyu, SUN Wenjun. Luminescence properties of Eu³⁺ doped CaMoO₄ micron phosphors[J]. Acta Physica Sinica, 2015, 10: 287-295.
赵聪, 孟庆裕, 孙文军. Eu³⁺掺杂CaMoO₄微米荧光粉发光性质的研究[J]. 物理学报, 2015, 10: 287-295.
- [10] WANG Fei. Preparation and luminescent properties of phosphor Sr₂La₈(SiO₄)₆O₂:Eu^(2+,3+)[J]. Acta Photonica Sinica, 2018, 47(8): 0816001.
王飞. Sr₂La₈(SiO₄)₆O₂:Eu^(2+,3+)荧光粉的制备和发光性能[J]. 光子学报, 2018, 47(8): 0816001.
- [11] SREELEKSHMI A K, LAL S C, GANESANPOTTI S. Probing the multifunctionality of double layered perovskite NaGdMgTeO₆:Eu³⁺ in ratiometric phosphor thermometry and solid-state lighting[J]. Journal of Alloys and Compounds, 2022, 905:164138.
- [12] TOBY B H, VON DREELE R B. GSAS-II: the genesis of a modern open-source all purpose crystallography software package[J]. Journal of Applied Crystallography, 2013, 46(2): 544-549.
- [13] TAUC J, GRIGOROVICI R, VANCU A. Optical properties and electronic structure of amorphous germanium [J]. Physica Status Solidi (b), 1966, 15(2): 627-637.
- [14] SURAJA N J, MAHESH A, SIBI K S, et al. Insights into the crystal structure and multifunctional optical properties of A₂CdTeO₆ (A=Ba, Sr, Ca) double perovskites[J]. Journal of Alloys and Compounds, 2021, 865:158902.
- [15] YE Ying, WANG Linxiang, TUO Juan, et al. Preparation and luminescence properties of metal ions Li⁺, Na⁺ and Al³⁺ co-doped BaF₂:Eu³⁺ phosphors[J]. Acta Photonica Sinica, 2018, 47(6): 0616003.
叶颖, 王林香, 屠娟, 等. 金属离子Li⁺、Na⁺、Al³⁺掺杂的BaF₂:Eu³⁺荧光粉的制备及发光特性[J]. 光子学报, 2018, 47(6): 0616003.
- [16] CAO C, YANG H K, MOON B K, et al. Hydrothermal synthesis, phase evolution, and optical properties of Eu³⁺-doped KF-YF₃ system materials[J]. Journal of Materials Research, 2012, 27(23): 2988-2995.
- [17] YU R, WANG C, CHEN J, et al. Photoluminescence characteristics of Eu³⁺-doped double-perovskite phosphors [J]. ECS Journal of Solid State Science and Technology, 2014, 3(3): 33-37.
- [18] SEKULIĆ M, DRAMIĆANIN T, ĆIRIĆ A, et al. Photoluminescence of the Eu³⁺-activated Y_xLu_{1-x}NbO₄ (x = 0, 0.25, 0.5, 0.75, 1) solid-solution phosphors[J]. Crystals, 2022, 12(3): 427.
- [19] LIU Q, WANG L, HUANG W, et al. Thermally stable double perovskite CaLaMgSbO₆:Eu³⁺ phosphors as a tunable led-phosphor material[J]. Ceramics International, 2018, 44(2): 1662-1667.
- [20] LI K, LIAN H, VAN DEUN R, et al. A far-red-emitting NaMgLaTeO₆:Mn⁴⁺ phosphor with perovskite structure for indoor plant growth[J]. Dyes and Pigments, 2019, 162: 214-221.
- [21] ZHANG X, ZHOU L, PANG Q, et al. Tunable luminescence and Ce³⁺→Tb³⁺→Eu³⁺ energy transfer of broadband-excited and narrow line red emitting Y₂SiO₅: Ce³⁺, Tb³⁺, Eu³⁺ phosphor[J]. The Journal of Physical Chemistry C, 2014, 118(14): 7591-7598.
- [22] CHANG Y, LIANG C, YAN S, et al. Synthesis and photoluminescence characteristics of high color purity and brightness Li₃Ba₂Gd₃(MoO₄)₈:Eu³⁺ red phosphors[J]. The Journal of Physical Chemistry C, 2010, 114(8): 3645-3652.
- [23] HE J, GAO Z, LIU S, et al. New Eu³⁺-activated bismuthate tellurate LiSrBiTeO₆ red-emitting phosphor for InGaN-based w-LEDs[J]. Journal of Luminescence, 2018, 202: 7-12.
- [24] LIANG J, ZHAO S, YUAN X, et al. A novel double perovskite tellurate Eu³⁺-doped Sr₂MgTeO₆ red-emitting phosphor with high thermal stability[J]. Optics & Laser Technology, 2018, 101: 451-456.
- [25] LI L, CHANG W, CHEN W, et al. Double perovskite LiLaMgWO₆:Eu³⁺ novel red-emitting phosphors for solid state lighting: synthesis, structure and photoluminescent properties[J]. Ceramics International, 2017, 43(2): 2720-2729.
- [26] LIU Wei, LI Zhuxin, WANG Junjie, et al. Regulation of electroluminescent properties of ZnO/GaN light emitting diodes by Er³⁺ doping[J]. Chinese Journal of Luminescence, 2021, 42(6): 863-870.
刘威, 李竹新, 王俊洁, 等. Er³⁺掺杂对ZnO/GaN发光二极管电致发光性能的调控[J]. 发光学报, 2021, 42(6): 863-870.
- [27] FERHI M, BOUZIDI C, HORCHANI-NAIFER K, et al. Judd-ofelt analysis of spectroscopic properties of Eu³⁺ doped KLa(PO₃)₄[J]. Journal of Luminescence, 2015, 157: 21-27.
- [28] ZHONG J, GAO H, YUAN Y, et al. Eu³⁺-doped double perovskite-based phosphor-in-glass color converter for high-power warm w-LEDs[J]. Journal of Alloys and Compounds, 2018, 735: 2303-2310.
- [29] LI X, LIU Q, HUANG W, et al. Structural and luminescent properties of Eu³⁺-doped double perovskite BaLaMgNbO₆

- phosphor[J]. *Ceramics International*, 2018, 44(2): 1909–1915.
- [30] DU P, YU J. Eu³⁺-activated La₂MoO₆-La₂WO₆ red-emitting phosphors with ultrabroad excitation band for white light-emitting diodes[J]. *Scientific Reports*, 2017, 7(1): 11953.
- [31] RAGHU T, RAJU D, RATNAKA C. Photoluminescence investigations of Eu³⁺-doped LiPbB₅O₉ as a red emitting phosphor for warm w-LED applications[J]. *Indian Journal of Physics*, 2021, 96(5): 1547–1558.
- [32] DU P, RAN W, LI W, et al. Morphology evolution of Eu³⁺-activated NaTbF₄ nanorods: a highly-efficient near-ultraviolet light-triggered red-emitting platform towards application in white light-emitting diodes[J]. *Journal of Materials Chemistry C*, 2019, 7(35): 10802–10809.

Preparation and Luminescent Properties of Red-emitting Y₆TeO₁₂:Eu³⁺ Phosphor

LI Rongqing, ZHOU Weiwei, TONG Yue, ZHENG Qinghua, LV Zhaocheng, ZHAO Wang,
XIA Zhengrong, LIU Fangfang

(School of Electrical Engineering, Huainan Normal University, Huainan 232038, China)

Abstract: The industry of white light-emitting diodes, next-generation illumination sources, has become an interesting field for their superior advantages such as energy savings, high efficiency, long operating lifetime as well as environmental friendliness. By far, the most effective white light-emitting diode is a combination of a near-ultraviolet chip and yellow-emitting phosphors. However, this type of phosphor converted white light-emitting diode has some disadvantages, it suffers from the weakness of low color rendering index and high correlated color temperature because of the deficiency of red component. Thus, to overcome this problem, a large number of red phosphors, especially the trivalent Eu³⁺ doped phosphor, have been widely studied. Eu³⁺ ion is an important red activator in most of the commercial red phosphors, which can provide an efficient and narrow band emission due to characteristic 4f-4f transitions. Especially, Eu³⁺ ions can be used to prove the point group symmetry of the substituted site in the host. When Eu³⁺ ions occupy noncentrosymmetric lattice sites, Eu³⁺ can emit intense red emission, benefiting to improve the overall efficiency of the white light-emitting diodes. So the host can affect the intensity of emission peaks of Eu³⁺ ion. Tellurate exhibits excellent properties in the optical, physical, and chemical fields. Given the low phonon energy of tellurate, this material can avoid the competitive non-radiative decay for the Eu³⁺ ions doped. Therefore, tellurate is suitable for hosting matrices used in phosphors. We report herein, the preparation and luminescent properties of red-emitting (Y_{1-x})₆TeO₁₂:xEu³⁺ phosphor. The (Y_{1-x})₆TeO₁₂:xEu³⁺ phosphors were prepared through the high-temperature solid-state reaction at 1200 °C for 20 h. The (Y_{1-x})₆TeO₁₂:xEu³⁺ phosphors were prepared in this way for seven different concentrations of Eu³⁺ (x=0.1, 0.2, 0.3, 0.4 and 0.5). The samples (Y_{1-x})₆TeO₁₂:xEu³⁺ were analyzed in detail by XRD, excitation and emission spectra, concentration quenching, thermal stability, luminescent decay curves, quantum efficiency, and color coordinates. To identify the detailed crystal structure information of (Y_{1-x})₆TeO₁₂:xEu³⁺ phosphors, the Rietveld refinement was performed using the Generalized Structure and Analysis System. The absence of an impurity phase in the present doping concentration ranges (0.1≤x≤0.5) confirmed that incorporation of Eu³⁺ ions did not show any notable change in Y₆TeO₁₂ phase. The refinement results were clear that the as-obtained (Y_{1-x})₆TeO₁₂:xEu³⁺ phosphors were of trigonal structure with R3(No.146) space group. Further representative particle distribution and scanning electron microscopy of the (Y_{0.7})₆TeO₁₂:0.3Eu³⁺ phosphors were carried out and the results indicate that average grain size is 4.61 μm with diameter ranging from 2 μm to 8 μm. The band gap energy E_g of (Y_{0.7})₆TeO₁₂:0.3Eu³⁺ obtained from diffuse reflectance spectra is 3.25 eV. The excitation and emission spectra of (Y_{1-x})₆TeO₁₂:xEu³⁺ phosphors show that the prepared phosphor can be excited by ultraviolet light (393 nm) or blue light (464 nm), and exhibits a strong red light emission band at 632 nm corresponding to ⁵D₀→⁷F₂ electric dipole transition of Eu³⁺ ions. The intensity ratio R of ⁵D₀→⁷F₂ to ⁵D₀→⁷F₁ transition ($R=I(^5D_0 \rightarrow ^7F_2)/I(^5D_0 \rightarrow ^7F_1)$) is a good way to measure the symmetry of Eu³⁺ sites. The intensity ratio value R is calculated to be 6.338. It is higher than some reported Eu³⁺-doped phosphors. Usually, with the increase of magnitude of R, the ideal value of the color chromaticity is closer. The dependence of integrated intensity on Eu³⁺ contents

reveals the optimum doping concentration is $x=0.3$, beyond which concentration quenching was observed. Concentration quenching for the prepared $(Y_{1-x})_6TeO_{12}:xEu^{3+}$ phosphors confirmed that the electric dipole–electric dipole interaction was responsible for energy transfer, resulting in the concentration quenching. The integrated emission intensity of prepared phosphor $(Y_{0.7})_6TeO_{12}:0.3Eu^{3+}$ at 150°C is as high as 76.5% of that at ambient temperature. The thermal activation energy was obtained as 0.196 9 eV, which ensures a good thermal stability. This demonstrates its possible application in solid state lighting or optical thermometry. The decay characteristics of $(Y_{1-x})_6TeO_{12}:xEu^{3+}$ phosphors were studied to understand the average lifetime of an activator ion in an excited state. The decay curves of the prepared $(Y_{1-x})_6TeO_{12}:xEu^{3+}$ phosphors were monitored under 393 nm excitation wavelength and 632 nm emission wavelength. At doping concentrations of Eu^{3+} , the luminescence lifetimes are 1 114 μs , 907 μs , 813 μs , 661 μs and 583 μs , respectively. The lifetime decreases with an increase in Eu^{3+} dopant concentration. This type of observation is results when the distance between the dopant Eu^{3+} ion decreases and this leads to nonradiative transitions. Based on the datum of emission spectrum of $(Y_{0.7})_6TeO_{12}:0.3Eu^{3+}$, the chromaticity coordinates are determined to be (0.637 6, 0.343 1), close to the National Television System Committee value (0.67, 0.33). To further evaluate the potential applications of the $(Y_{0.7})_6TeO_{12}:0.3Eu^{3+}$ phosphor, the prototype light-emitting diodes fabricated by coating the phosphors on the near-UV chips emit a bright light. The strong emission band (360~440 nm) originates from the near-UV chip and other sharp emission bands attribute to the Eu^{3+} 4f-4f transitions. The phosphor exhibits favorable luminescent properties, thermal stability of luminescence with good chromaticity coordinate, which have potential application in white light-emitting diodes.

Key words: $(Y_{1-x})_6TeO_{12}:xEu^{3+}$; Luminescent properties; Concentration quenching; Thermal stability; w-LED

OCIS Codes: 160.2100; 160.2540; 160.4670; 160.5690